

Rethinking sampling topologies for image quality estimation in Computational Imaging system design

Kathrin Berkner
Ricoh Innovations, Inc.
Menlo Park, California 94025
Email: berkner@rii.ricoh.com

Abstract—Optical design includes an optimization process that evaluates image degradations caused by the lens design in each iteration. In joint digital-optical imaging system design the optimization cost function needs to include measured image quality after optical and digital processing. A commonly used merit function is the mean-squared-error (MSE) of the digital image after restoration. Low resolution rectangular sampling grids increase the speed of the optimization process, but cause approximation errors of the MSE merit function. Through adaptation of the MSE calculations to flexible non-rectangular sampling topologies, we achieve increased MSE accuracy and significant speed-up of the processing time.

I. INTRODUCTION

Computational Imaging (CI) is a design framework for imaging system design that balances the processing capabilities of optics and electronics through concurrent design and joint optimization of all elements [1]. As a consequence, a CI system design distributes the process of image formation over the optics, detector, and the digital post-processing. Following the trend pioneered by [2] of designing digital-optical image system by exploring cooperative interaction between optical, detector, and digital processing subsystems for features such as extended depth of field, new methods for jointly optimizing both the optical and the digital subsystems based on the linearity of the corresponding filter subsystems have been proposed recently [3]. Therein, the performance of a digital-optical system including Wiener filter restoration is evaluated by propagating the object source information through the complete digital-optical imaging system in two steps: (a) through the optical system via wave propagation, and (b) through the digital system via linear filtering for deblurring. Using a cost function based on this system propagation for individual system component optimization has lead to novel system designs and functionalities, e.g. the one proposed in [3] [4]. In computer simulation such joint optimization requires efficient and accurate sampling of the analog optical and the discrete digital domain.

The baseline implementation to achieve the designs in [3][4] was done using rectangular sampling grids for both domains. Even though the final designs look promising, the design process was very time consuming since the computational complexity of the joint performance evaluation was slow and provided not always accurate solutions. In order to make the end-to-end system design process practicable for an industrial system designer, the simulation tool needs to achieve speed

and accuracy similar to traditional optical-only and digital-only design tools.

In this paper we describe details of new sampling strategies recently introduced in [5] to efficiently sample performance metrics that measure the end-to-end system performance, describe how to set sampling parameters for an example system design space, and report experiments on computational complexity and accuracy of the proposed approximation.

II. REQUIREMENTS FOR CI SYSTEM DESIGN

In order to design a computational imaging system, not just the captured data at the sensor, but desired output information of the end-to-end system needs to be evaluated, and system components optimized for best end-to-end performance. In the case of a photographic imaging system, scene information needs to be propagated through optical components onto the detector, converted to digital data and further processed by a digital processor to produce an image acceptable for the human visual system. The system performance metric has to be defined such that it can be used as a cost function in an optimization framework that optimizes optical characteristics (e.g. shapes of lenses, choices of glass, number of elements), as well as digital processing characteristics (e.g. filter responses).

Before considering practical implementation issues of a system performance metric, we first review the image formation process of a digital-optical imaging system as well as a specific performance metric for end-to-end system design and its integration into system design optimization.

A. Image formation in digital-optical systems

The optical part of the image formation is described by wave propagation through optical elements, in our case lenses, whereas the digital part is described by signal processing algorithms. In the following we briefly review both image formation steps.

A planar wave front passing through a lens is described by the *generalized pupil function* P_λ , defined as

$$P_\lambda(x, y) = P_0(x, y) \exp(ik\Phi(x, y)),$$

where P_0 is the pupil function describing the finite extend of the lens, $k = 2\pi/\lambda$ is the *wave number*, and Φ is the *optical path different (OPD)*, describing the deviation of the actual wavefront from an ideal reference sphere [6].

Assuming a lens with focal length f and a transparent pupil, and an object at infinity, the wave front at the image forming plane can be approximated by the Fraunhofer approximation of the diffraction integral, given by

$$U_\lambda(u, v) = \frac{1}{i\lambda f} \int \int_{-\infty}^{\infty} P_\lambda(x, y) \exp \left[i \frac{k}{f} (xu + yv) \right] dx dy,$$

which is proportional to the Fourier transform \mathcal{F} of P_λ . The resulting optical system is typically characterized by its point-spread-function (PSF), H , given by

$$H = |U_\lambda|^2, \text{ with } U_\lambda \propto \mathcal{F}(P_\lambda), \quad (1)$$

and its *optical transfer function (OTF)*, \mathcal{H} , by

$$\mathcal{H} = \mathcal{F}(H) = \mathcal{F}(|U|^2). \quad (2)$$

The digital image \mathbf{y} of a sampled source spectral radiance $\mathbf{x}(\lambda)$, passing through an optical system with OTF $\mathcal{H}_{\lambda, f}$, and captured by a photodetector with spectral response $d(\lambda)$, can now be modeled by

$$\mathbf{y} = \int d(\lambda) \mathbf{H}_\lambda \mathbf{x}(\lambda) d\lambda + \mathbf{n},$$

where \mathbf{H}_λ represents the sampled point-spread function for the system, and \mathbf{n} represents the random noise introduced by the detector.

In a photographic imaging system, the detector's response is split into different color channels (e.g. red, green, blue). For this case, we can model a signal in color channel c as

$$\mathbf{y}_c = \mathbf{h}_c \mathbf{x}_c + \mathbf{n}, \quad (3)$$

where \mathbf{h}_c represents the sampled point-spread function for color channel c [4].

Digital post-processing steps may be performed to enhance the quality of the captured signal by removing image degradations such as blur or noise. In this paper we follow [3] and consider the Wiener filter for image restoration. Given a blur filter \mathbf{f} with Fourier transform F and the power spectral densities S_z of the input signal z and S_n of the noise \mathbf{n} , the Wiener filter is given by $G = \frac{F}{|F|^2 + S_n/S_z}$. The final estimated image data \tilde{z} of the input signal z results in $\tilde{z} = \mathbf{f} * z$.

Given the optical propagation model described earlier, we model the blur filter \mathbf{f} to be the sampled PSF \mathbf{h}_c from (3) with Fourier transform $\hat{\mathbf{h}}_c$. The Wiener filter for restoration of the signal \mathbf{y}_c , is then

$$G_c = \frac{\hat{\mathbf{h}}_c}{|\hat{\mathbf{h}}_c|^2 + S_n/S_x}. \quad (4)$$

B. Image system quality evaluation

In traditional optical system design, the optical image quality is measured by a metric operating on the wavefront error, the PSF, or the OTF. One commonly used measure is the *root-mean-squared error of the optical path difference (RMS-OPD)*, measuring the amount of wavefront error introduced by the lens expressed using the OPD function Φ :

$$\text{RMS-OPD} = \|\Phi\|_{L_2}. \quad (5)$$

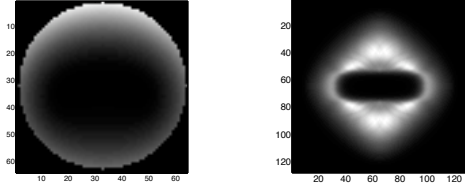


Fig. 1. Example of the OPD (left) and Wiener filter error prediction S_e (right) for the singlet example analyzed in Section IV for aberration values $w_{20} = -2.75$, $w_{astig} = 1.4089$, $w_{coma} = -1.2602$, $w_{spherical} = 1.5578$, $w_{fc} = 2.7198$.

Digital image quality, in contrary, is often measured by the *mean-squared-error (MSE)* between the ideally sampled signal $\tilde{\mathbf{y}}$ and the estimated digital image samples $\hat{\mathbf{y}}$:

$$\text{MSE}(\tilde{\mathbf{y}}, \hat{\mathbf{y}}) = E[\|\hat{\mathbf{y}} - \tilde{\mathbf{y}}\|^2]. \quad (6)$$

When measuring the end-to-end performance of a digital-optical system, it is not enough to consider only the optical quality. The quality measure needs to operate on the restored digital data, including the optical image formation and digital processing into the estimation. For that purpose, a *joint system MSE measure, JMSE*, has been defined [3] as

$$\text{JMSE}(u) = \frac{1}{2\pi} \int \int_{|\omega_1| < u, |\omega_2| < u} S_e(\omega_1, \omega_2) d\omega_1 d\omega_2, \quad (7)$$

where

$$S_e(\omega_1, \omega_2) = \frac{S_x(\omega_1, \omega_2) S_n(\omega_1, \omega_2)}{|\hat{\mathbf{h}}_c(\omega_1, \omega_2)|^2 S_x(\omega_1, \omega_2) + S_n(\omega_1, \omega_2)}, \quad (8)$$

is the error spectral density of the Wiener filter from Eq. (4) with $\hat{\mathbf{h}}_c$ being the OTF of the optical system, S_x the signal source model, S_n the detector noise model, and u the Nyquist frequency of the sensor.

C. Joint optimization of digital-optical system

Optimization of a digital-optical system is traditionally performed by first optimizing the optical subsystem using a lens design software. That software executes a large number of iterations in search of an optimal design each computing optical quality measures for adjusted glass parameters. For such optimization optical quality measures have to be computed often more than 1000 times before a design of sufficient quality is found. Performing the system optimization jointly for optical and digital subsystems with respect to end-to-end system quality, the JMSE function has to be evaluated instead of an optical metric. This JMSE cost function needs to interface with the optical design software such that it causes adjustment of the glass parameters to a solution that predicts optimal system quality after digital restoration. In contrast to traditionally optimized optical designs with a typical RMS-OPD $\leq \frac{1}{10} \lambda$, the RMS-OPD value inherent to CI systems might be quite large ($\geq 3\lambda$), since aberrations in the optics are allowed and compensated for via digital processing. Figure 1 shows the OPD and the S_e error for a highly aberrated optical

system. Large OPD values of 3.5 cluster at the boundary of the pupil. Large values of the restoration error S_e (white) correlate to zeros of the OTF of the optical system.

III. JMSE APPROXIMATION

For approximation of the JMSE through computer simulation, the analog optical signal needs to be sampled. For traditional optical system design simulation, the digital computation of RMS-OPD is extremely efficient taking advantage of the representation of the OPD in terms of orthogonal polynomials [6] and accurate numerical integration using Gauss quadrature techniques [7], [8]. Most field locations require tracing fewer than 20 rays per field location to the pupil, i.e. need to evaluate less than 20 samples of the OPD.

Computation of the JMSE function implies sampling of the S_e error function which required two Fourier transform computations, one for the PSF, Eq.(1), and one for the OTF, Eq. (2). Then numerical integration over the S_e samples in the region restricted by the sensor Nyquist frequency u Eq. (7) needs to be performed.

In the following we analyze different sampling strategies for OPD and S_e domains with respect to approximation accuracy and computational efficiency.

A. Square-grid sampling strategy

Our baseline sampling strategy uses the FFT algorithm for the Fourier transforms and a simple rectangle rule for the integration. For this strategy, we start with a $B \times B$ square-grid-sampling of the OPD. To compute the OTF, FFT operations are applied to a zero-padded two-dimensional array on a $2B \times 2B$ grid. Finally, the JMSE is calculated by performing a rectangular-rule integration of the error function S_e within the sampling band of the system which is of size $2B \cdot u \times 2B \cdot u$, where $u = \frac{\omega_N}{\omega_D}$ is the ratio of the sampling frequency divided by the diffraction-limited spatial frequency ω_D .

In practice, we typically need to trace at least 64^2 rays to the pupil for each field location. This sampling rate is driven by the numbers of samples required for the numerically stable integration of S_e over a hypercube of aberrations. For $B = 64$, the available $(128 \cdot 0.2)^2 = 25^2$ equally spaced grid samples barely provide a dense enough sampling of S_e around the critical zeros in the OTF to compute numerically stable JMSE approximation, especially for small values of u . The average execution time for one iteration computing the JMSE for $B = 64$ is 10 sec, compared to 5 msec for computation of the optical-only RMS-OPD measure. This increased execution time makes the JMSE-based optimization be not practical for every-day use by an imaging system designer.

B. Numerical integration of S_e via quadratures

When applying the square-grid sampling strategy, we notice that we have to compute a large number of S_e samples in order to obtain dense sampling at the zeros of the OTF, but then ignore the samples at frequencies larger than u during the integration. That leads to the idea of choosing sampling locations depending on function characteristics of S_e and on

the Nyquist frequency u . To include regularity information of S_e into the placement of the integration nodes, we choose numerical quadratures for the integration step.

Numerical integration via quadrature approximates the integral over a function f as a finite sum of weighted function values of f at certain locations: $\int_a^b f(x)dx \approx \sum_{k=1}^p w_k f(x_k)$. The locations x_k are called *nodes* and the parameters w_k *weights* of the quadrature of *order* p . If the integrand can be written as $f(x) = g(x)W(x)$ where $g(x)$ is approximately polynomial and $W(x)$ is known, then the nodes are linked to zeros of certain orthogonal polynomials. The most popular type of quadrature is the Gauss quadrature. In this case $W(x) = 1$, $[a, b] = [-1, 1]$, and the nodes are zeros of Legendre polynomials being independent of the integrand function f . The accuracy of the approximation depends on the smoothness of the function f . If f is a polynomial of order $2p$, then a Gaussian quadrature of order p is enough to represent the integral exactly. More details on quadrature integration can be found, e.g. in [9].

When trying to apply the quadrature approach to the integration of S_e we need to consider the smoothness of the integrand function. Whereas the noise spectrum is assumed to be constant and the signal spectrum to be at least one times differentiable in the integration interval, the modulation transfer function $|\hat{h}_c|$ is continuous, but may not be everywhere differentiable. Therefore, we can not expect that a low order quadrature will give acceptable results. This lack of smoothness is typically not inherent to the optical-only OPD function. That latter function has an efficient polynomial approximation through the Zernike expansion, whereas S_e can not be assumed to be at least one times differentiable. Therefore, we investigate in this paper experimentally, what order of polynomial approximation of S_e is necessary to yield acceptable results (see Section IV).

For integration via quadrature we need to evaluate the integrand function at the quadrature node locations. These locations may differ from the ones provided by the FFT applied to the original square grid samples of the OPD and PSF. To solve this problem we apply the non-equally spaced FFT (NFFT) [10] to compute the OTF at the quadrature node locations.

C. Polar sampling of the OPD

Ray tracing to pupil locations intersecting a dense grid of size $B \times B$ with $B \geq 64$ has been identified as the main reason for the slow performance for the baseline JMSE sampling strategy [5]. Our goal is, therefore, to reduce the number of OPD values obtained via ray tracing by changing the sampling grid topology to one that is more suitable for capturing OPD information while still maintaining good system accuracy. In order to achieve that goal we apply a concept already used to calculate merit functions for purely optical systems, namely sampling the OPD values on a polar grid of L rings and K arms [7]. The polar grid sampling strategy has been shown appropriate for efficiently sampling the OPD on the pupil, since the OPD is typically represented by a few lower

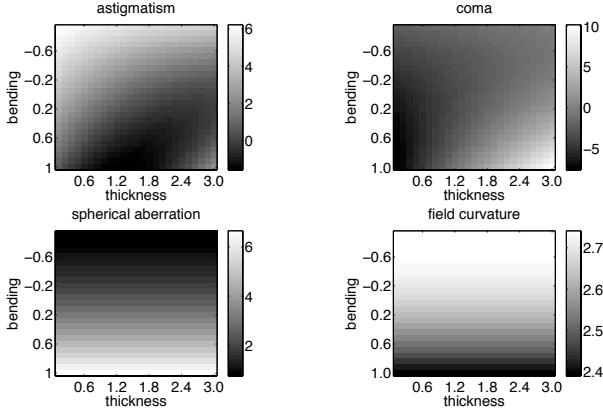


Fig. 2. Aberration space of the singlet design for astigmatism, coma, spherical aberration, and field curvature.

order optical aberrations, which are modeled as polynomials in radius and angle.

D. Other approaches

Other approaches of approximating not the JMSE, but the PSF include approximating the generalized pupil function with a Taylor approximation (e.g. [11]). This approach is efficient for small wave front errors. For large errors, however, too many Taylor expansion terms are needed to provide good approximation due to the fact that the Taylor series is expanded around the optical axis, but the wave front error for highly aberrated system is more concentrated at the boundary of the pupil (see Fig. 1).

Fourier transforms on polar grids have been studied recently by [12], [13]. The grids used in these papers all have a higher sampling density towards the origin of the grid, i.e. near the optical axis, and sparse sampling towards the edge of the sampling region, i.e. towards the boundary of the pupil, whereas we need more samples towards the pupil boundary to capture highly aberrated OPDs.

An interesting approach for approximation of transforms on band-limited functions in a disc has been presented by [14]. The authors link the Fourier transform on a band-limited function on a disc to a certain eigenvalue problem. It would be very interesting to analyze whether it is possible to adapt this approach to the computation of digital-optical quality measures. But such analysis is beyond the scope of this paper.

IV. EXPERIMENTS

At the example of a singlet we estimate what sampling of the OPD function is necessary to provide a good approximation of the OPD for large aberrations, then analyzing what quadrature is suitable for providing a numerically stable JMSE approximation.

The singlet is the simplest lens design consisting only of one lens element, parameterized by thickness and curvature. We choose this design with F-number of 4.6 to evaluate parameter settings for the quadrature-based JMSE approximation. The

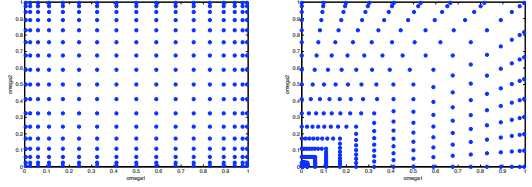


Fig. 3. Grids for different numerical quadratures of order $p = 16$ in the first quadrant: nodes for Gauss quadrature in both dimensions (left), nodes for Gauss quadrature in radial and trapezoidal rule in angular dimension (right).

thickness of surface one is in the range of 0 to 3 mm sampled at 25 equally spaced locations. The curvature on surface 2 is in the range of -0.1 to 0.1 (in inverse mm), sampled at 25 equally spaced locations. The aberrations for the design space are extracted using the lens design software Zemax in terms of the aberrations astigmatism, coma, spherical aberration, and field curvature, as well as defocus. These aberrations sampled over the design space are shown in Fig. 2. We notice that the aberrations have very large values (> 5) compared to aberrations observed in traditional optical system design (less than 2). These large aberrations can be characteristic for computational imaging systems that restore optically introduced degradations via digital processing. For each sample location in the five-dimensional hypercube of aberrations, we compute the OPD at pupil locations on a polar grid with L rings and K arms. In order to measure the accuracy of the sampling, we first compute "ground truth" OPD values $OPD_{64 \times 64}$ for locations on a high-density square-grid of size 64×64 , which serves as a reference grid, and then compare these data with the OPD values $OPD_{L \times K \rightarrow 64 \times 64}$ interpolated from the polar $L \times K$ grid to the quadratic 64×64 reference grid via bi-cubic interpolation. The OPD error over the entire design space we define now as

$$d_{\Omega}[K, L] = \int_{\Omega} \|OPD_{64 \times 64}(w) - OPD_{L \times K \rightarrow 64 \times 64}(w)\|_{L^2} dw, \quad (9)$$

where Ω is the aberration hypercube. Figure 4 shows results using this two error measure for a field location of $h = 0.95$ of the singlet design space. OPD differences are measured via $d_{\Omega}[K, L]$ for various polar grids $L = 2, \dots, 10, K = 4, \dots, 32$ resulting in $N = L \cdot K$ total number of samples. A general rule of thumb in traditional optical design is that the RMS-OPD error should be $\leq \frac{1}{10}\lambda$ for an acceptable optical design. Using this rule of thumb, we choose the parameters $L = 6$ and $K = 40$ that achieve an estimated OPD error $\leq \frac{1}{10}\lambda$ for $N = 240$ total samples.

The accuracy of integration of S_e is analyzed using different numerical integration techniques. For the baseline square-grid strategy, first 128^2 S_e samples have to be computed. Then a simple rectangle rule is applied to $(128 \cdot u)^2$ samples having a fixed grid spacing independent of u . That implies that for small u only very few samples are included in the integration. Two integration methods using different non-rectangular grid

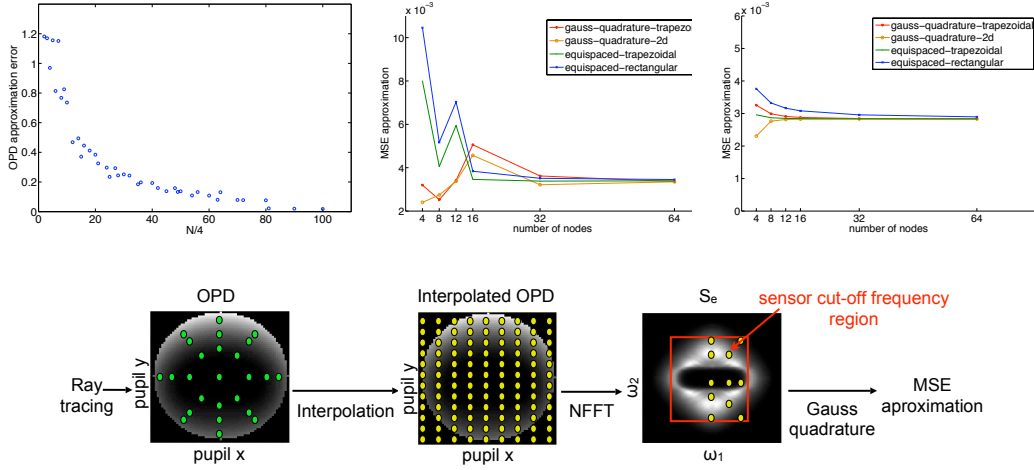


Fig. 4. Top: OPD approximation error d_{Ω} measured for $n = 64$ (left), and accuracy of proposed JMSE approximation for different integration methods and two different defocus locations -6.0 (middle) and -2.75 (right). Bottom: Schematic overview of proposed sampling strategy for computing the JMSE measure for optimization of CI systems.

topologies are considered: (a) performing a Gauss quadrature integration in both dimensions of the integral, and (b) performing a Gauss quadrature in the radial and a trapezoidal-rule integration method in the angular dimension. The number of integration nodes for all methods varies between $p = 4$ and 64 for one quadrant in the S_e plane. Figure 3 shows the sampling grids for those to integration strategies.

For $u = 0.2$, the JMSE is calculated for different defocus locations -2.75 , and -6.0 , where -2.75 is close to and -6.0 far away from the optimal defocus location in the considered design space. The computed JMSE values are shown in Fig. 4 and demonstrate that at defocus location away from the optimal location the equispaced rectangular and trapezoidal methods show unstable behavior for small number of nodes. In comparison, the Gauss quadrature-based methods show a more stable behavior. This observation explains the accuracy problems occurring with the current implementation at small u -values implying an under-sampling of the relevant S_e region. Close to the optimal defocus location all methods perform similarly. We conclude that a quadrature of order $p = 16$, resulting in $2p^2 = 512$ S_e -samples for two quadrants, provides acceptable JMSE approximation accuracy. For comparison, for the baseline strategy implementation, 128^2 S_e -samples on an equispaced grid need to be computed.

The computational efficiency of the proposed sampling strategy was first tested in a stand-alone C-implementation and then integrated into the Zemax lens design software. The predicted speed-up of 20x was confirmed in practical experiments for more complicated lens designs including multiple lens elements and elements with aspheric shapes.

V. CONCLUSIONS

We have introduced a new sampling strategy for computing the JMSE merit function, an MSE-based merit function including optical system characteristics suitable for the optimization of joint digital-optical imaging systems. The proposed strategy

overcomes the accuracy and complexity problems of the baseline implementation by including non-rectangular sampling grids for the OPD and Wiener filter error estimator domains and NFFT operations to propagate information between those domains. The achieved speed-up of 20x makes the implementation applicable for use with professional lens design software for practical system designs.

REFERENCES

- [1] J. N. Mait, "A History of Imaging: Revisiting the Past to Chart the Future," *Optics and Photonics News*, vol. 17, pp. 22–27, 2006.
- [2] E. R. Dowski and W. T. Cathey, "Extended depth of field through wavefront coding," *Applied Optics*, vol. 34, no. 11, pp. 1859–1866, 1995.
- [3] David Stork, M. Dirk Robinson, "Theoretical Foundations for joint digital-optical analysis of electro-optical imaging systems," *Applied Optics*, Vol. 47, Issue 10, pp. B64-B75, vol. 47, no. 10, pp. B64–B75, 2008.
- [4] M. D. Robinson and D. Stork, "Joint digital-optical design of imaging systems for grayscale objects," in *Proceedings of the SPIE European Optical Design Conference*, Sept. 2008.
- [5] K. Berkner and M. D. Robinson, "Non-rectangular sampling topologies for fast joint digital-optical system optimization," in *Proceedings of the OSA Computational Optical Sensing and Imaging*, October 2009.
- [6] M. Born and E. Wolf, *Principles of Optics*, Pergamon Press, 1991.
- [7] G. W. Forbes, "Optical system assessment for design: numerical ray tracing in the Gaussian pupil," *J. Opt. Soc. Am.*, vol. 5, no. 11, pp. 1943–1956, 1988.
- [8] Z. D. Corporation, "ZEMAX User's Guide," 2004.
- [9] W. Press et al., *Numerical Recipes*, Cambridge University Press, 2007.
- [10] D. Potts et al., "Fast Fourier transforms for nonequispaced data: A tutorial," *Modern Sampling Theory: Mathematics and Applications*, pp. 249–274, 2001.
- [11] S. Bagheri et al., "Reduced-complexity representation of the coherent point-spread function in the presence of aberrations and arbitrarily large defocus," *Journal of the Optical Society of America*, vol. 23, no. 10, pp. 2476–2493, 2006.
- [12] A. Averbuch et al., "Fast and accurate Polar Fourier transform," *Appl. Comput. Harmon. Anal.* 21, vol. 21, pp. 145–167, 2006.
- [13] M. Fenn et al., "On the computation of the polar FFT," *Applied and Computational Harmonic Analysis*, vol. 22, pp. 257–263, 2007.
- [14] G. Beylkin et al., "Grids and transforms for band-limited functions in a disc," *Inverse Problems*, vol. 23, pp. 2059–2088, 2007.